JOURNAL OF MATERIALS SCIENCE 30 (1995) 5944–5952

Excimer laser and electron beam irradiation effects in iron-doped lithium niobate

M.SORESCU‡, E. T. KNOBBE, J. J. MARTIN,*
*Departments of Chemistry and *Physics, Oklahoma State University, Stillwater, OK 74078–0447, USA*

J. D. BARRIE
Mechanics and Materials Technology Center, The Aerospace Corporation, M2/248, P.O. Box 92957, Los Angeles, CA 90009–2957, USA

D. BARB
Institute of Atomic Physics, P.O. Box MG/7, R-76900 Bucharest, Romania

Excimer laser ($\lambda = 308$ nm, $\tau = 10$ ns) and electron beam (W = 7 MeV) irradiation effects in $^{57}Fe:LiNbO_3$ have been studied on samples of two crystallographic orientations. Complementary information regarding radiation induced changes to the optical absorbance of the crystal, valence states of Fe, phase composition and morphology of the irradiated regions was obtained by optical absorption measurements, Mössbauer spectroscopy, scanning electron microscopy (SEM), energy dispersive X-ray (EDX) spectroscopy, microRaman and Read thin film camera analysis. The relationship between irradiation treatment conditions and induced property modifications in iron-doped lithium niobate is reported within the frame of available defect models.

1. Introduction

Crystalline lithium niobate exhibits interesting piezoelectric, pyroelectric, electrooptic, and non-linear optical properties. In its ferroelectric phase, the $LiNbO_3$ structure has an $R3c$ space group and is based on an approximate hexagonal packing of oxygen atoms. All three cationic sites (the Li site, the Nb site and a vacant site) have distorted octahedral coordination by oxygen to give C_3 point symmetry. Doping with transition metal atoms markedly influences the optical properties of lithium niobate. In the $LiNbO_3$ structure, Fe impurities probably substitute for Li cations [1], although a small fraction positioned at the Nb or intrinsic vacant sites cannot be ruled out. Despite the fact that iron in the Fe^{2+}–Fe^{3+} system is generally recognized as one of the main active impurities, the role of structural defects responsible for the photorefractive effect is not yet understood [2–12].

Due to its relation to optical damage, the photorefractive effect is of particular importance with regard to the use of lithium niobate as a substrate material for preparation of optical waveguides and hybrid optoelectronic devices [13]. Since lithium niobate is not easily processed by conventional mechanical or chemical techniques, laser ablation is increasingly being used for micromachining, fashioning reticulated waveguiding structures, direct writing of optoelectronic circuits, and for the deposition of thin films on semiconductor substrates [14]. In order to optimize these processes, the relationship between irradiation parameters and laser induced property changes in the lithium niobate crystal has to be ascertained [15].

Moreover, electron beam irradiation of undoped lithium niobate has been found to represent a promising approach to obtaining correlation between certain point defects and their corresponding absorption bands [6]. From this viewpoint, electron beam irradiation of $^{57}Fe:LiNbO_3$ is expected to provide a deeper understanding of the types and chemistry of structural defects formed in its crystalline lattice, due to the presence of Mössbauer probe nuclei.

In order to obtain new information on the fundamental effects underlying the interaction of excimer laser and electron beams with $^{57}Fe:LiNbO_3$, radiation-driven modifications and microstructure evolution during irradiation are studied in the present work by optical absorption measurements, Mössbauer spectroscopy, SEM, EDX, microRaman and Read thin film camera analysis. Correlations between radiation induced changes to structural and optical properties of iron-doped lithium niobate are discussed in the light of available defect models.

2. Experimental procedure

2.1. Sample preparation

$^{57}Fe:LiNbO_3$ single crystal doped with 0.22% Fe_2O_3, 95% enriched in ^{57}Fe was congruently grown from the melt by the Czochralski technique. Platelets with the plane parallel and, respectively, perpendicular to the c-axis were cut from the bulk crystal.

‡*Present address*: Duquesne University, Department of Physics, 430 Mellon Hall, Pittsburgh, PA 15282-1503, USA.

0022–2461

Samples of 0.2 mm thick for Mössbauer measurements were obtained by mechanical polishing.

Iron-doped lithium niobate platelets were further exposed to the $\lambda = 308$ nm radiation generated by a XeCl excimer laser (Lambda Physik), having the pulse width at half maxima, $\tau = 10$ ns. Single pulse energy densities of $w = 40$ mJ mm^{-2} (known to be above the ablation threshold) were achieved by focusing with a cylindrical fused silica lens to a spot size of about 0.25×10 mm^2. Samples with both crystallographic orientations were isochronally irradiated with 10 and 20 laser pulses per spot at 100 mJ pulse^{-1} and a repetition rate of 10 Hz. Laser beam scanning of the sample surface, which was placed on an x–y–z micrometer translation stage [16–18], resulted in a reticulated structure of the irradiated areas with a characteristic spacing of 0.25 mm. All specimens were irradiated in air at room temperature.

A different set of ^{57}Fe:LiNbO$_3$ platelets was subjected to high energy electron beam irradiation. The electrons had an energy, $W = 7$ MeV and radiation doses of 50 and 200 Mrad were employed.

2.2. Experimental techniques

Optical absorption measurements of as-grown, laser treated and electron irradiated ^{57}Fe:LiNbO$_3$ samples were performed using a Cary 2400 spectrophotometer, covering the wavelength range from 350 to 800 nm.

Room temperature transmission Mössbauer measurements were made with a constant acceleration spectrometer (Ranger Scientific). The 25 mCi γ-ray source was ^{57}Co in a rhodium matrix, maintained at room temperature. Mössbauer spectra of as-grown, laser treated and electron irradiated ^{57}Fe:LiNbO$_3$ platelets of both crystallographic orientations were collected with incident gamma rays perpendicular to the plane of the samples.

SEM investigations were performed using a Jeol electron microscope at 25 keV, operating in the secondary electron emission mode. In order to avoid charging effects, the samples were sputtered coated with gold–palladium.

Raman microanalysis was performed on an Instruments S.A. Ramanor U-1000 spectrometer, coupled to an Olympus research grade microscope. Laser excitation was via an argon ion laser (Coherent 305) operating at 488 nm. The laser power incident on the sample was about 30 mW. The incident laser light was polarized, but the polarization state of the scattered radiation was not analysed. The beam was focused to a spot size of approximately 1 μm, allowing measurement of Raman scatter from small features within the damaged regions. Signals were detected using a cooled GaAs photomultiplier (Hamamatsu) and collected in 180° scattering geometry. To improve signal-to-noise ratios, several scans were recorded and averaged. The spectrometer resolution was 1.8 cm^{-1}, much less than the intrinsic line widths of the collected spectra.

X-ray diffraction data were obtained with a Read thin film camera using nickel filtered copper radiation. The X-ray beam was orientated at an angle of 15° from the plane of the sample.

3. Results and discussion

3.1. Optical absorption measurements

Fig. 1 a shows the optical absorption spectra of the ^{57}Fe:LiNbO$_3$ crystal in the as-grown state (curve 1) and after pulsed excimer laser irradiation (curves 2 and 3). Despite some persisting controversy [2–12], one can regard as reliable the inference that the main absorption bands in the spectrum of undoped lithium niobate in the as-grown state are located around 480, 390 and 750 nm (2.6, 3.2 and 1.6 eV, respectively). They are most likely due to two-electron oxygen vacancies (F centres), singly ionized oxygen vacancies (F^+ centres) and the (Nb^{4+}) electron–polaron state, respectively. In doped lithium niobate crystals, however, additional absorption bands are present, which are associated with electron transitions to the higher lying energy levels of the impurity centres. In particular, the absorption band around 500 nm (2.5 eV) is associated with the intervalence transition $Fe^{2+} \rightarrow Nb^{5+}$, while an electron transition from the valence band to the Fe^{3+} level is accompanied by optical absorption in the 400 nm (3.1 eV) band [19].

As a result of pulsed excimer laser irradiation ($\lambda = 308$ nm, $\tau = 10$ ns, E = 100 mJ pulse^{-1}) with 10 pulses per spot at a repetition rate of 10 Hz, the iron-doped lithium niobate samples were observed to become a dark grey colour. Fig. 1 a shows a corresponding growth in the optical absorbance of the ^{57}Fe:LiNbO$_3$ crystal, as a result of the laser treatment performed (curve 2). The increased absorption of the ^{57}Fe:LiNbO$_3$ samples can be associated with the occurrence of reduction effects (and the corresponding increase in the Fe^{2+} concentration), the formation of structural defects due to laser irradiation and the onset of laser induced changes in surface stoichiometry. Furthermore, it can be seen in Fig. 1 a, for the ^{57}Fe:LiNbO$_3$ platelet irradiated with 20 laser pulses per spot, that the rapidly saturating growth in the optical absorbance extends over the whole visible range and exhibits no clearly discernible features (curve 3). This plot also suggests that a higher concentration of defect centres is formed in the sample irradiated with an increased number of laser pulses per spot. Consequently, the laser induced changes to the optical absorption of the ^{57}Fe:LiNbO$_3$ samples are found to depend on the values of the irradiation parameters. One may note that a wide absorption band (from 350 to 700 nm), similar to that observed in the present excimer laser irradiation study, was reportedly produced by irradiating the lithium niobate crystal with γ quanta, X-rays or neutrons [19–21].

Fig. 1 b shows the optical absorption spectra of the ^{57}Fe:LiNbO$_3$ samples in the as-grown state (curve 1), and after 7 MeV electron beam irradiation at radiation doses of 50 and 200 Mrad (curves 2 and 3, respectively). The observed dose dependent changes to optical absorption induced by fast electron irradiation suggest an increased intensity of the polaron absorption band at 750 nm at the expense of the short wavelength part of the spectrum. These radiation driven modifications are consistent with a decrease in the concentration of both Fe^{2+} and Fe^{3+}, as well as F and F^+ centres.

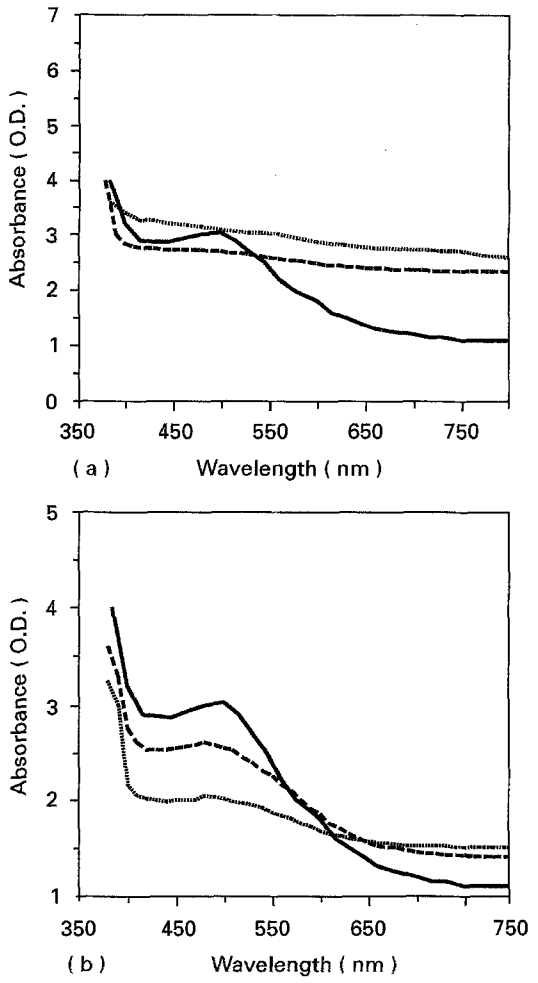

Figure 1 (a) Excimer laser induced effects ($\lambda = 308$ nm, $\tau = 10$ ns) on the optical absorption spectra of $^{57}Fe:LiNbO_3$. — Curve 1, as-grown crystal; (- - -) curve 2, after 10 laser pulses per spot; (···) curve 3, after 20 laser pulses per spot. (b) Electron beam irradiation effects ($W = 7$ MeV) in the optical absorption spectra of $^{57}Fe:LiNbO_3$. — Curve 1, as-grown crystal; (- - -) curve 2, after 50 Mrad; (···) curve 3, after 200 Mrad.

In order to correlate the changes in optical absorbance to structural and morphological modifications induced by excimer laser and electron beam irradiation of $^{57}Fe:LiNbO_3$, the use of complementary investigation techniques is necessary.

3.2. Mössbauer spectroscopy measurements

Fig. 2 a,d shows the room temperature transmission Mössbauer spectra of the as-grown $^{57}Fe:LiNbO_3$ crystal, recorded with the γ-ray propagation direction parallel and, respectively, perpendicular to the crystallographic c-axis. Both spectra are dominated by two quadrupole split doublets. The corresponding values of the quadrupole splittings and isomer shifts: $\Delta E_Q = 0.42 \pm 0.1$ mm s^{-1}, $\delta = 0.37 \pm 0.05$ mm s^{-1} and $\Delta E_Q = 1.79 \pm 0.01$ mm s^{-1}, $\delta = 1.05 \pm 0.05$ mm s^{-1} indicate the presence of high spin Fe^{3+} and Fe^{2+} valence states, respectively. The determined values of the hyperfine parameters are in good agreement with previously reported data on $^{57}Fe:LiNbO_3$ absorbers obtained by diffusion enrichment [22]. The Fe^{3+} concentration in the as-grown lithium niobate crystal (estimated to be 70% of the iron dopant) explains the broad absorption feature superimposed in the room temperature Mössbauer spectra. This feature is characteristic of slow electronic relaxation between the three crystal field states (Kramers doublets) of the $^6S_{5/2}$ ion [23–25]. The $|\pm 1/2>$ states of Fe^{3+} are known to relax faster than the other two electronic states at the same temperature [26], and account for the partially resolved quadrupole doublet present in the spectra shown in Fig. 2.

The quadrupole doublet corresponding to Fe^{2+} ions shows an angular dependence of the line intensity ratio consistent with a local environment of axial symmetry (vanishing asymmetry parameter), lattice vibrational isotropy (absence of Goldanskii–Karyagin effect) and thin absorber approximation (no saturation effects). Indeed, under these assumptions the relative intensity of the $\Delta m = \pm 1$ line to the $\Delta m = 0$ line of the quadrupole doublet is given by [27]

$$R_q = (3/2)\,(1 + \cos^2\theta)/[1 + (3/2)\sin^2\theta]$$

where θ is the angle between the direction of the electric field gradient, V_{ZZ}, and the γ-ray propagation direction. Consequently, extreme line intensity ratios of 3:1 and 3:5 are expected in the cases of parallel ($\theta = 0°$) and perpendicular ($\theta = 90°$) orientations of the γ-ray direction and the direction of V_{ZZ}. The relative line intensities observed in the spectra of Fig. 2a,d for $^{57}Fe:LiNbO_3$ platelets of both crystallographic orientations clearly illustrate these predictions.

Room temperature Mössbauer spectra of $^{57}Fe:LiNbO_3$ samples exposed to pulsed excimer laser irradiation ($\lambda = 308$ nm, $\tau = 10$ ns, $E = 100$ mJ pulse^{-1}) with 10 and 20 laser pulses per spot at a repetition rate of 10 Hz are shown in Fig. 2b,e corresponding to the γ-ray propagation direction parallel and perpendicular to the crystallographic c-axis, respectively. Analysis of the relative line intensities indicates a 1% increase in the Fe^{2+} versus Fe^{3+} concentration, corresponding to a slight overall reduction of the lithium niobate samples under the laser treatment conditions used. Considering the high heating and cooling rates associated with excimer laser irradiation [16, 17], this result is not unexpected, since rapid quenching from high temperatures typically results in an overall oxygen deficiency and the corresponding formation of Fe^{2+} ions in these systems [28]. One may note that the same iron percentage was reportedly converted to Fe^{2+} upon 10 h irradiation with $\lambda = 366$ nm from a high pressure Hg lamp [29].

Consequently, compared to the as-grown crystal, a small increase in the Fe^{2+} versus Fe^{3+} concentration was determined by the present Mössbauer spectroscopy measurements on laser irradiated $^{57}Fe:LiNbO_3$ samples. However, since the optical absorption band related to Fe^{2+} ions [19] is located at 500 nm (2.5 eV), the increased optical absorbance over the whole visible range observed in Fig. 1 a for the laser treated platelets cannot be assigned to reduction effects only. These results suggest that irradiation induced defect centres and a modified surface stoichiometry play an important role in explaining the

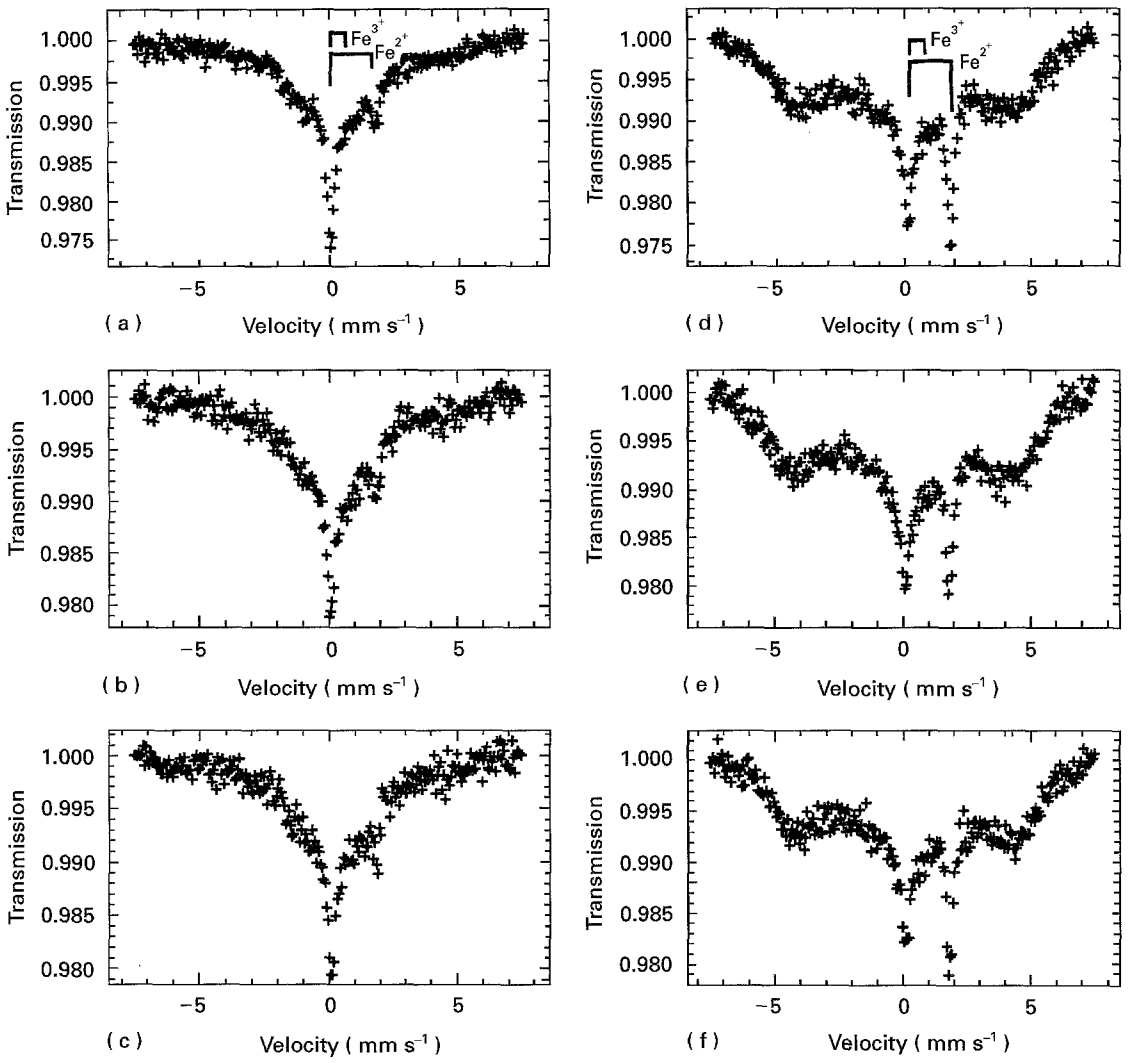

Figure 2 Room temperature transmission Mössbauer spectra of $^{57}Fe:LiNbO_3$ crystal, recorded with the γ-ray propagation direction parallel (a–c) and perpendicular (d–f) to the crystallographic *c*-axis, respectively. (a,d) as-grown; (b,e) after pulsed excimer laser irradiation with 10 pulses per spot; (c,f) after pulsed excimer laser irradiation with 20 pulses per spot.

increased optical absorption of excimer laser treated iron-doped lithium niobate samples.

For irradiation by 308 nm laser pulses, $h\nu \sim E_{gap}$. One photon absorption produces free electrons and holes, which subsequently may recombine or be trapped. The formation of small polarons through capture of electrons (by Nb^{5+} ions) and holes (by O^{2-} ions or lithium vacancies) is accompanied by lattice distorsions. While vacancy and interstitial defects are produced in the bulk, these lattice perturbations may initiate ionic motion at the microscopic scale, such that a Nb polaron may be transferred to a lithium ion site. Indeed, the assignment of the broad absorption band peaking at 750 nm (1.6 eV) to the (Nb_{Li}^{4+}) bound small polaron has been recently confirmed unambiguously by optically detected magnetic resonance techniques [10]. The increased intensity of the polaron absorption band due to ultra violet (u.v.) laser irradiation observed in Fig. 1a partially accounts for the observed optical absorption spectrum of the iron-doped lithium niobate samples. Most of the underlying optical absorption, however, is due to the wide absorption band (from 350 to 700 nm) originating in reduced, laser ablated regions and related to heavy lattice rearrangements. Complementary information on the occurrence of laser induced morphological and stoichiometrical changes, obtained by SEM/EDX, microRaman and Read thin film camera analysis of the excimer laser irradiated iron-doped lithium niobate samples are presented in the next sections.

Fig. 3a shows the room temperature transmission Mössbauer spectrum of the as-grown $^{57}Fe:LiNbO_3$ sample, recorded in a narrow velocity range with the γ-ray propagation direction parallel to the crystallographic *c*-axis. Fig. 3b,c shows the Mössbauer spectra of iron-doped lithium niobate platelets exposed to 7 MeV electron beams at radiation doses of 50 and 200 Mrad, respectively. The dramatic decrease in the resonant absorption area obtained from the Mössbauer spectra of electron irradiated samples is consistent with displacement of some iron ions to a lattice site exhibiting a reduced recoilless fraction for the ^{57}Fe probe nuclei (presumably, intrinsic vacant sites or interstitial positions). This correlates with the decrease in the concentration of both Fe^{3+} and Fe^{2+} centres, responsible for the 400 and 500 nm bands in

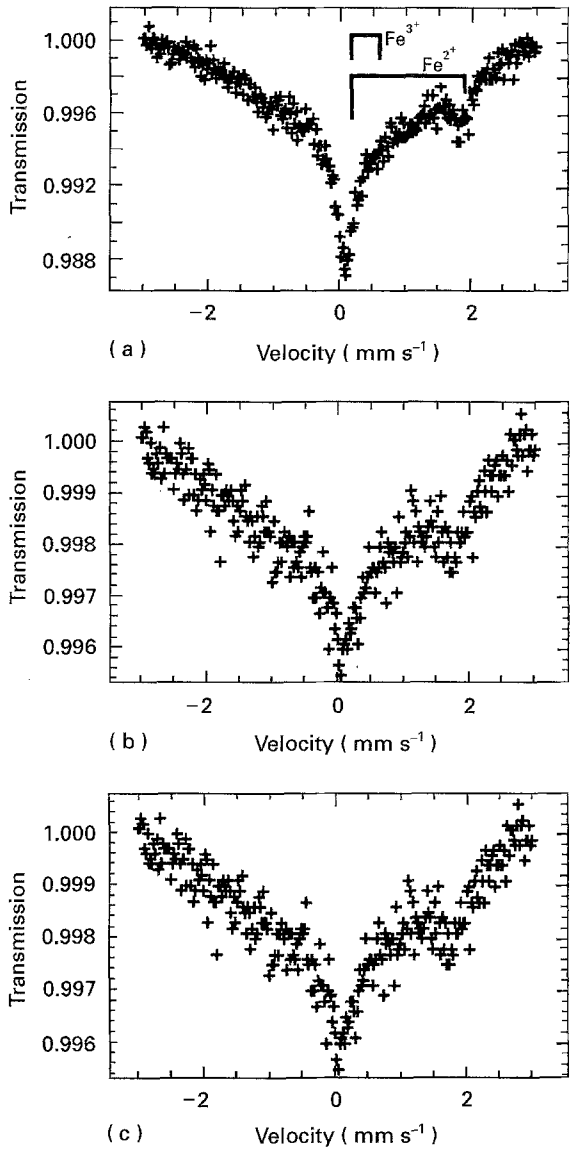

Figure 3 Room temperature transmission Mössbauer spectra of $^{57}Fe:LiNbO_3$, recorded with the γ-ray propagation direction parallel to the crystallographic *c*-axis: (a) as-grown, (b) after 7 MeV electron beam irradiation with a radiation dose of 50 Mrad, and (c) after 7 MeV electron beam irradiation with a radiation dose of 200 Mrad.

the optical absorption spectra of iron-doped lithium niobate samples, as inferred from Fig. 1b. On the other hand, it is known that oxygen vacancies near Fe or a change in the coordination number of iron should result in a broader distribution of hyperfine parameters [27]. Therefore, the increased widths of the resonance lines in the Mössbauer spectra of the electron irradiated $^{57}Fe:LiNbO_3$ samples (Fig. 3b,c), corresponding to a distribution of quadrupole splittings and isomer shifts, suggest the occupation of several inequivalent lattice sites by the iron ions, as an effect of radiation induced displacement damage. Indeed, the energy of the fast electrons used in the present irradiation study is known to be higher than the 1 MeV energy threshold for the formation of defects in the lithium niobate structure, due to atomic displacement [6, 18]. As in the case of laser irradiated samples, heavy lattice rearrangements account for the broad band in the visible, underlying the optical absorption spectrum of electron beam irradiated $^{57}Fe:LiNbO_3$ samples (Fig. 1b). In addition, the dose dependent decrease in the absorption bands corresponding to *F* type centres and simultaneous increase in the intensity of the polaron absorption band at 750 nm indicate ionization of the F centres and selfcapture of the freed electrons onto Nb^{5+}. This transfer process between radiation induced bands is similar to the behaviour of optical absorption bands produced by thermal reduction and further supports previously reported results on the formation of oxygen vacancy centres in undoped lithium niobate due to ionizing radiation [6, 19].

3.3. SEM/EDX investigations

In order to gain additional information on the structural and morphological changes responsible for the increased absorbance of the laser damaged $^{57}Fe:LiNbO_3$ crystalline samples, SEM examinations of the laser treated surfaces have also been performed (Fig. 4a–c). They reveal the presence of a reticulated structure, consisting of alternating light and dark regions, located at the edges and centre of the laser irradiation area, respectively. The dark zones (denoted as D zones in Fig. 4c) penetrate deeper inside the laser irradiated surface, indicating the occurrence of ablation related effects. For the 308 nm laser radiation [14], the absorption coefficient is $\alpha \sim 250\ cm^{-1}$, such that an exponential absorption profile versus depth results and 99% of the photons are absorbed in a thickness of $\sim 200\ \mu m$.

Intriguing features regarding the morphology of the laser ablated regions, which exhibit a black appearance due to oxygen deficiency [30], can be observed in Fig. 5a. The SEM micrograph shows the formation of pores and cracks on the irradiated surface. The presence of pores in the laser ablated regions is particularly relevant for demonstrating intense gas circulation through the sample surface during laser treatment. Indeed, it has been recently suggested that in the ablation regime, oxygen is sputtered preferentially from the lithium niobate sample [14], such that oxygen vacancies and a modified stoichiometry may result in the near surface region. Moreover, the surface modifications resulting in the formation of cracks in the laser treated platelets indicate that the reduced regions formed as an effect of pulsed excimer laser irradiation should contribute to the strong background (Fig. 1a) in the optical absorption spectrum of the laser damaged $^{57}Fe:LiNbO_3$ crystal.

It can be seen in the SEM examinations of Figs 4c and 6a, that the light regions (denoted as B-zones) formed at the edges of the laser impact area are characterized by the presence of micrometre size crystallites, corresponding to the phases formed during the laser induced melt vaporization and recrystallization phenomena. Moreover, a distinctive surface morphology is exhibited by the zones separating the laser recrystallized from the laser ablated regions (and denoted by C-zones in Fig. 4c). EDX analysis of select microvolumes in the irradiated zones typically showed a 5% increase in the Nb content of the recrystallized

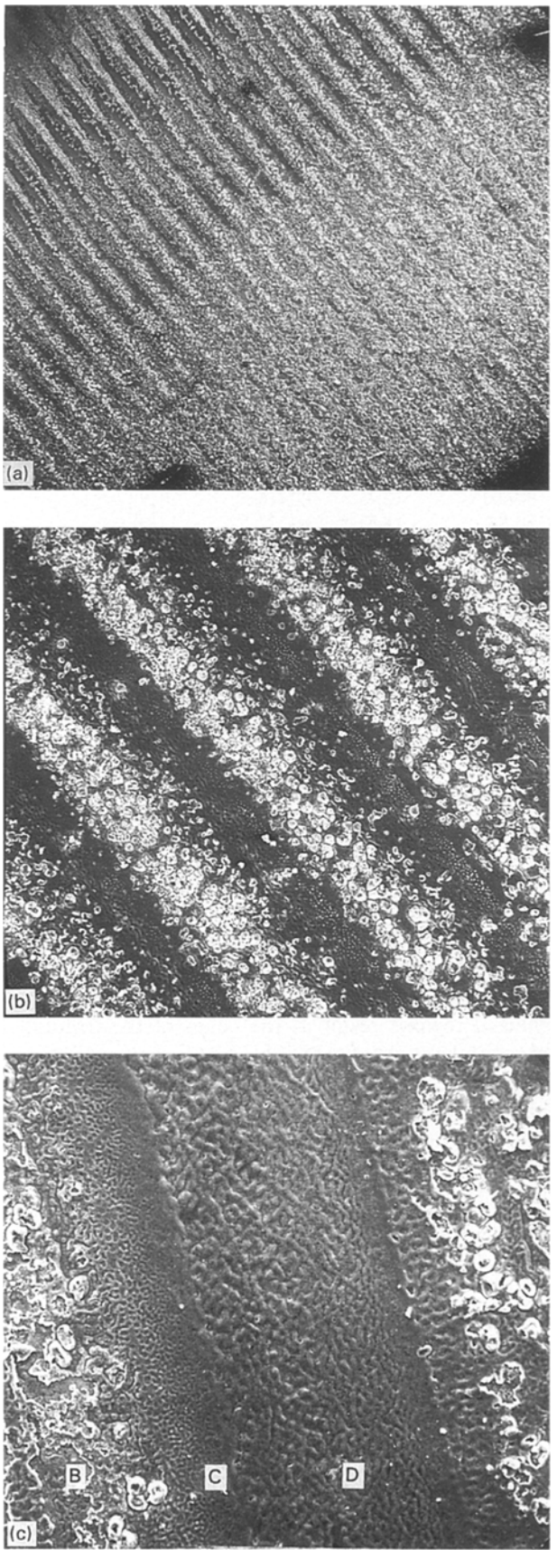

Figure 4 SEM examinations of $^{57}Fe:LiNbO_3$ crystal, after pulsed excimer laser irradiation ($\lambda = 308$ nm, $\tau = 10$ ns, $E = 100$ mJ pulse^{-1}, repetition rate 10 Hz) with 20 pulses per spot. The magnification employed had the values: (a) $\times 20$, (b) $\times 100$, and (c) $\times 200$.

areas (Fig. 6b), as compared to the laser ablated regions (Fig. 5b). Consequently, in order to characterize further the laser induced modifications to surface

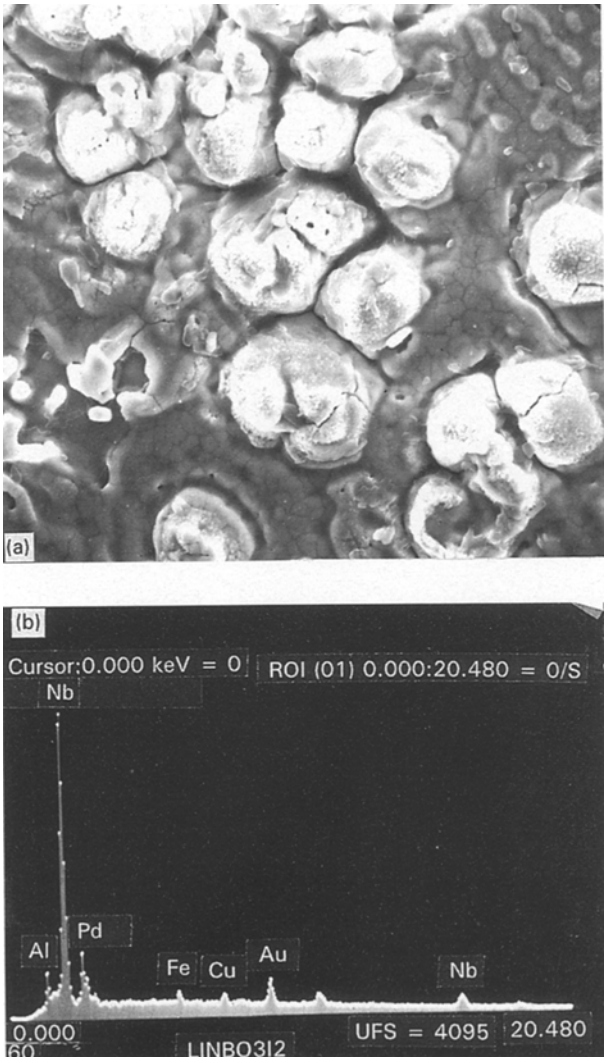

Figure 5 (a) SEM photograph ($\times 3600$) and (b) EDX examination of the laser ablated regions formed in the $^{57}Fe:LiNbO_3$ crystal by pulsed excimer laser irradiation. The Nb and Fe peaks correspond to the crystal; Al and Cu impurities come from the holder and tape, whereas Au and Pd peaks represent the coating.

stoichiometry and nature of the recrystallized phases formed as an effect of the excimer laser treatment performed, the investigations recognized the use of microRaman and Read thin film camera analysis for probing select areas in the irradiated regions.

3.4. MicroRaman and Read thin film camera analysis

The Raman spectra corresponding to the as-grown and excimer laser irradiated $^{57}Fe:LiNbO_3$ crystal are shown in Fig. 7a–d. Raman microanalysis of the laser exposed platelets was performed at different locations of the irradiated areas relative to the centre of the laser impact zone. Thus, Fig. 7b shows the Raman spectrum of a microcrystallite formed in the laser recrystallized regions. Raman microanalysis of this surface feature is indicative of trigonal lithium niobate. The observed line broadening as compared to the Raman spectrum of the non-irradiated sample (Fig. 7a) suggests the occurrence of quenching stresses, originating in the high heating and cooling rates associated with pulsed excimer laser irradiation.

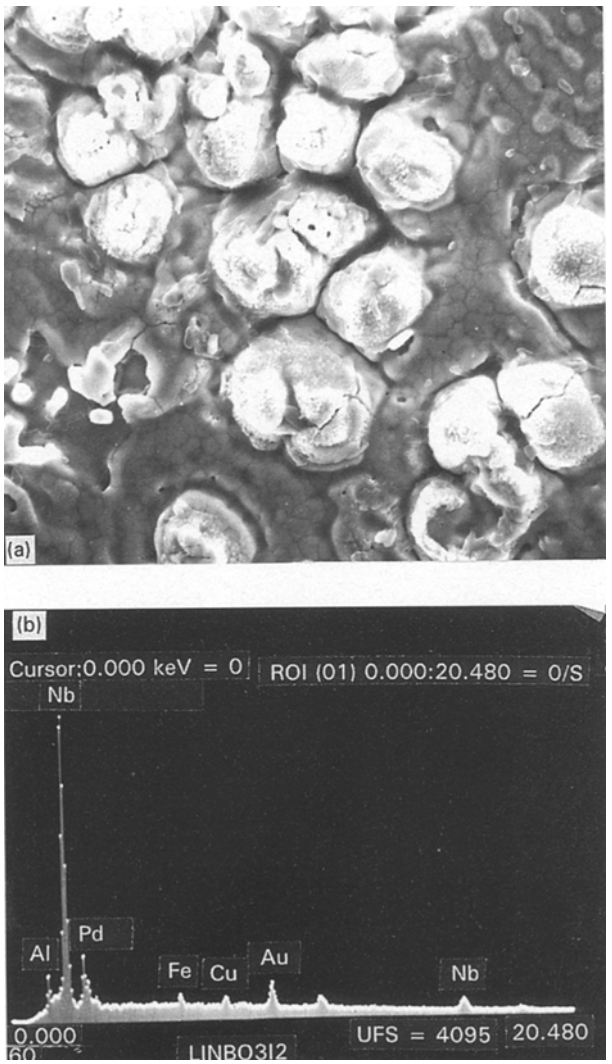

Figure 6 (a) SEM photograph (× 800) and (b) EDX examination of the recrystallized regions formed in the $^{57}Fe:LiNbO_3$ crystal by pulsed excimer laser irradiation. The Nb and Fe peaks correspond to the iron-doped lithium niobate sample.

The Raman spectra taken at the margins and centre of the laser ablated regions are shown in Fig. 7c,d, respectively. They are indicative of niobate materials, with characteristic bands in the 580–630 cm^{-1} and 850–900 cm^{-1} region. However, these spectra exhibit additional bands which cannot be assigned to trigonal $LiNbO_3$. X-ray diffraction data obtained by Read thin film camera analysis (Table I) indicate that the additional phases formed as a result of the excimer laser treatment performed exhibit a textured polycrystalline component and can be assigned [31] to Li_7NbO_6 and Nb_2O_5, the latter occurring in noticeably smaller amounts. On these grounds, the different niobium partitioning inferred from EDX analysis of the laser ablated and laser recrystallized areas (Figs 5b and 6b) is attributable to an unequal distribution of lithium-rich niobate and niobium pentoxide phases.

4. Conclusions

Pulsed excimer laser irradiation ($\lambda = 308$ nm, $\tau = 10$ ns) of $^{57}Fe:LiNbO_3$ crystalline samples results in a significant increase in the optical absorbance over

TABLE I Read thin film camera analysis of pulsed excimer laser irradiated $^{57}Fe:LiNbO_3$ crystal

Distance (mm)	2θ (deg)	d-spacing (nm)	Estimated intensity (arbitary units)
48.650	24.45	0.3640	12.0
50.750	26.88	0.3320	20.0
56.450	33.46	0.2678	8.0
58.450	35.77	0.2511	100.0
60.150	37.73	0.2384	90.0
61.700	39.52	0.2280	12.0
62.350	40.27	0.2240	5.0
64.650	42.92	0.2107	8.0
69.750	48.81	0.1866	5.0
71.450	50.77	0.1798	5.0
72.900	52.45	0.1745	12.0
74.300	54.06	0.1696	8.0
76.800	56.95	0.1617	8.0
80.150	60.82	0.1523	20.0
84.600	65.95	0.1416	12.0
86.700	68.38	0.1372	8.0
95.500	78.54	0.1218	8.0
98.350	81.83	0.1177	8.0
102.300	86.39	0.1126	8.0
104.850	89.33	0.1097	8.0
122.900	110.17	0.0940	12.0
126.450	114.26	0.0918	20.0

the whole visible range, dependent on the number of applied laser pulses. As probed by the laser induced changes to the valence states of Fe, the modification of optical properties is accompanied, however, by a small global reduction of the lithium niobate crystal. Thus, irradiation induced point defects and surface modifications of the laser damaged areas are mainly responsible for the dramatic growth in optical absorbance of the irradiated lithium niobate samples. Laser recrystallized regions result at the edges of the irradiated areas and consist of trigonal $LiNbO_3$ microcrystals. In the centre of the laser impact zones, however, laser ablated regions are formed. These are characterized by the presence of Li_7NbO_6 and Nb_2O_5 crystalline phases. At the boundary of the laser recrystallized and laser ablated regions, trigonal $LiNbO_3$, Li_7NbO_6 and Nb_2O_5 crystalline phases are observed to coexist. Excimer laser irradiation has proven to be a powerful tool for studying non-conventional aspects of materials response by selectively inducing localized changes in the ferroelectric crystal under investigation. By the use of appropriate high resolution characterization techniques, fundamental effects underlying the interaction of excimer laser radiation with ferroelectric crystals were demonstrated in the present work on $^{57}Fe:LiNbO_3$: increased optical absorbance, reduction, ablation and laser induced recrystallization of multiple phases.

High energy electron beam irradiation ($W = 7$ MeV) of $^{57}Fe:LiNbO_3$ crystalline platelets was shown to induce dose dependent changes to optical absorption. The observed increase in the intensity of the polaron absorption band at the expense of the short wavelength part of the spectrum was found to be consistent with ionization of F centres and selfcapture of the freed electrons onto Nb^{5+}. Moreover, radiation induced displacement damage was demonstrated by

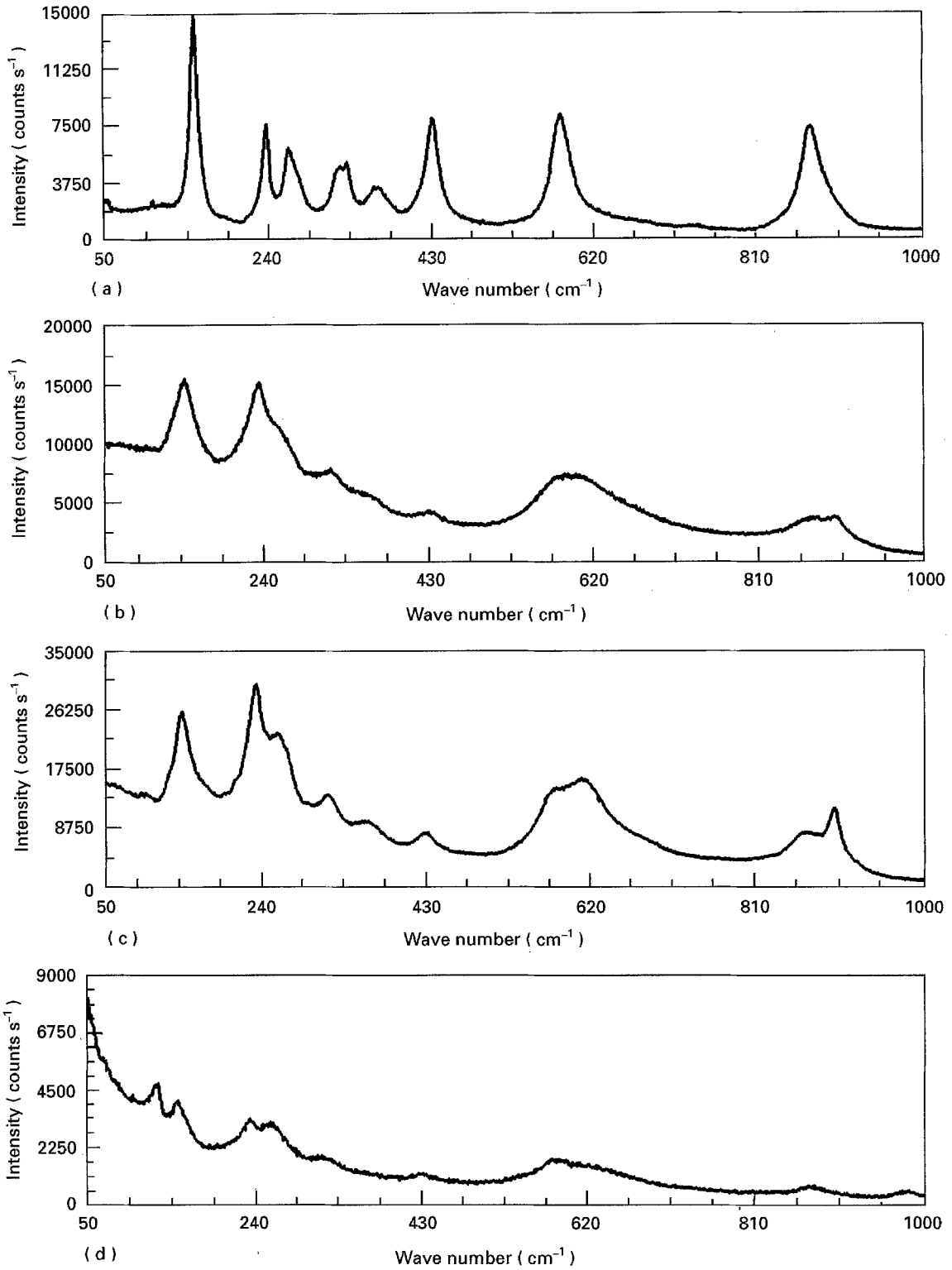

Figure 7 Raman microanalysis of $^{57}Fe:LiNbO_3$ performed at different locations of the irradiated areas relative to the centre of the laser impact zone: (a) non-irradiated crystal, (b) spectrum taken in a laser recrystallized region, (c) spectrum recorded at the boundary of a laser recrystallized and a laser ablated region, and (d) spectrum corresponding to a laser ablated region (see Fig. 4c for identification of the irradiated areas).

the observed decrease in the recoilless fraction and simultaneous broadening of the resonance lines in the Mössbauer spectra of electron irradiated $^{57}Fe:LiNbO_3$.

Acknowledgements

This work was sponsored by the National Science Foundation and the Office of Naval Research. Funding was also supplied by the Aerospace Sponsored Research Program. The authors are indebted to P. M. Adams for providing the X-ray data.

References

1. L. REBOUTA, M. F. DASILVA, J. C. SOARES, M. HAGEALI, J. P. STOQUERT, P. SIFFERT, J. A. SANZ-GARCIA, E. DIEGUEZ, and F. AGULLO-LOPEZ, *Europhys. Lett.* **14** (1991) 557.
2. H. JHANS, J. M. HONIG and C. N. R. RAO, *J. Phys. C* **19** (1986) 3649.

3. J. KOPPITZ, O. F. SCHIRMER and A. I. KUZNETSOV, *Europhys. Lett.* **4** (1987) 1055.
4. A. GARCIA-CABANES, E. DIEGUEZ, J. M. CABRERA and F. AGULLO-LOPEZ, *J. Phys.: Condens. Matter* **1** (1989) 6453.
5. P. J. JORGENSEN and R. W. BARLETT, *J. Phys. Chem. Solids* **30** (1969) 2639.
6. E. R. HODGSON and F. AGULLO-LOPEZ, *Solid State Commun.* **64** (1987) 965.
7. D. M. SMYTH, *Ferroelectrics* **50** (1983) 93.
8. G. G. DELEO, J. L. DOBSON, M. F. MASTERS and L. H. BONJACK, *Phys. Rev. B* **37** (1988) 8394.
9. A. P. WILKINSON, A. K. CHEETHAM and R. H. JARMAN, *J. Appl. Phys.* **74** (1993) 3080.
10. H. J. REYHER, R. SCHULTZ and O. THIEMANN, *Phys. Rev. B* **50** (1994) 3609.
11. N. ZOTOV, H. BOYSEN, F. FREY, T. METZGER and E. BORN, *J. Phys. Chem. Solids* **55** (1994) 145.
12. J. BLUMEL, E. BORN and T. METZGER, *ibid.* **55** (1994) 589.
13. M. A. McCOY, S. A. DREGIA and W. E. LEE, *J. Mater. Res.* **9** (1994) 2040.
14. M. AFFATIGATO, K. TANG, R. F. HAGLUND and C.H.CHIEN, *Appl. Phys. Lett.* **65** (1994) 1751.
15. M. SORESCU, J. D. BARRIE, J. J. MARTIN and E. T. KNOBBE, *Solid State Commun.* **94** (1995) 407.
16. M. SORESCU and E. T. KNOBBE, *Phys. Rev. B* **49** (1994) 3253.
17. M. SORESCU, E. T. KNOBBE and D. BARB, *ibid.* **51** (1995) 840.
18. M. SORESCU, E. T. KNOBBE, D. BARB, D. SORESCU and I. BIBICU, *Hyperfine Interact.* **92** (1994) 1347.
19. A. M. PROKHOROV and Y. S. KUZMINOV, "Physics and Chemistry of Crystalline Lithium Niobate" (Adam Hilger, Bristol, 1990) p. 94.
20. J. ROSA, K. POLAK and J. KUBATOVA, *Phys. Status Solidi (b)* **111** (1982) K85.
21. R. PAREJA, R. GONZALEZ and M. A. PEDROSA, *Phys. Status Solidi (a)* **84** (1984) 179.
22. W. KEUNE, S. K. DATE, I. DEZSI and U. GONSER, *J. Appl. Phys.* **46** (1975) 3914.
23. H. D. PFANNES and A. PUTZKA, *Hyperfine Interact.* **28** (1986) 785.
24. A. PUTZKA and H. D. PFANNES, *ibid.* **42** (1988) 1067.
25. H. D. PFANNES and A. PUTZKA, *ibid.* **56** (1990) 1477.
26. G. K. WERTHEIM and J. P. REMEIKA, *Phys. Lett.* **10** (1964) 14.
27. U. GONSER "Mössbauer Spectroscopy" (Springer-Verlag, New York, 1975) p. 29.
28. E. M. GYORGY, K. NASSAU, M. E. EIBSCHUTZ, J. V. WASZCZAK and C. A. WANG, *J. Appl. Phys.* **50** (1979) 2883.
29. H. ENGELMANN, W. GATZWEILER, I. DEZSI and U. GONSER, *Phys. Status Solidi (a)* **105** (1988) 219.
30. G. A. SMITH, L. C. CHEN and M. C. CHUANG, *Mater. Res. Soc. Symp. Proc.* **235** (1992) 843.
31. J. HAUCK, *Z. Naturforsch.* **24** (1969) 1067.

Received 17 March
and accepted 24 May 1995